Storm surge barrier performance

The effect of barrier failures on extreme water level frequencies

Mooyaart, L. F.; Bakker, A. M.R.; van den Bogaard, J. A.; Jorissen, R. E.; Rijcken, T.; Jonkman, S. N.

DOI
10.1111/jfr3.13048

Publication date
2024

Document Version
Final published version

Published in
Journal of Flood Risk Management

Citation (APA)
Mooyaart, L. F., Bakker, A. M. R., van den Bogaard, J. A., Jorissen, R. E., Rijcken, T., & Jonkman, S. N. (2024). Storm surge barrier performance: The effect of barrier failures on extreme water level frequencies. *Journal of Flood Risk Management*, *18*(1), Article e13048. https://doi.org/10.1111/jfr3.13048

Received: 2 January 2024 | Revised: 29 August 2024 | Accepted: 4 November 2024

DOI: 10.1111/jfr3.13048

ORIGINAL ARTICLE

CIWEM Chartered Institution of Water and Environmental Management | Journal of Flood Risk Management | WILEY

Storm surge barrier performance—The effect of barrier failures on extreme water level frequencies

L. F. Mooyaart[1,2] | A. M. R. Bakker[1,2] | J. A. van den Bogaard[3] | R. E. Jorissen[4] | T. Rijcken[1] | S. N. Jonkman[1,5]

[1]Faculty of Civil Engineering and Geosciences, Department of Hydraulic Engineering, Delft University of Technology, Delft, The Netherlands

[2]Department of storm surge barriers and guard locks, Rijkswaterstaat, Utrecht, The Netherlands

[3]Department of water Barriers, Rijkswaterstaat, Utrecht, The Netherlands

[4]Department of National Flood Defences, Rijkswaterstaat, Utrecht, The Netherlands

[5]Texas A&M Galveston, Galveston, Texas, USA

Correspondence
L. F. Mooyaart, Faculty of Civil Engineering and Geosciences, Department of Hydraulic Engineering, Delft University of Technology, Stevinweg 1, 2628 CN Delft, The Netherlands.
Email: l.f.mooyaart@tudelft.nl

Funding information
Directorate General of Public Works and Water Management (Rijkswaterstaat), the Netherlands

Abstract

Sea level rise necessitates the upgrade of coastal flood protection including storm surge barriers. These large movable hydraulic structures are open in normal conditions, but close during a storm surge to prevent coastal floods in bays and estuaries. Barrier improvements lower their susceptibility to operational, structural, or height-related failures. However, there is no method to determine the relative importance of these three barrier failure types. Here, we present a probabilistic method to systematically organize barrier failures and storm conditions to establish exceedance frequencies of extreme water levels behind the barrier. The method is illustrated by an assessment of extreme water level frequencies at Rotterdam (The Netherlands), which is protected by the Maeslant barrier. Four combinations of barrier states and storm conditions were analyzed and prioritized in the following order: (1) an operational failure with 1/100 year storm conditions, (2) a successful closure with an extreme (~1/1000 year) river discharge accumulating behind the barrier, (3) structural failure, and (4) insufficient height both with extreme storm conditions (10^{-6} year). The case study confirmed the method's ability to systematically explore promising barrier improvements to adapt to sea level rise, in this case, lowering the susceptibility toward operational failures.

KEYWORDS
flood defense, flood safety, storm surge barrier, system safety

1 | INTRODUCTION

Storm surge barriers are an important type of coastal flood protection as they protect coastal cities such as London (UK), New Orleans (USA), and Rotterdam (The Netherlands). These large barriers mitigate flood disasters by closing during storm surges while allowing tidal movements and navigation during normal conditions (Mooyaart & Jonkman, 2017).

Storm surge barriers are part of a larger flood protection system, which consists of an inner basin and interior flood defenses. These interior flood defenses are constituted of elevated land, flood walls and dikes, the latter which are also referred to as embankments (UK) and

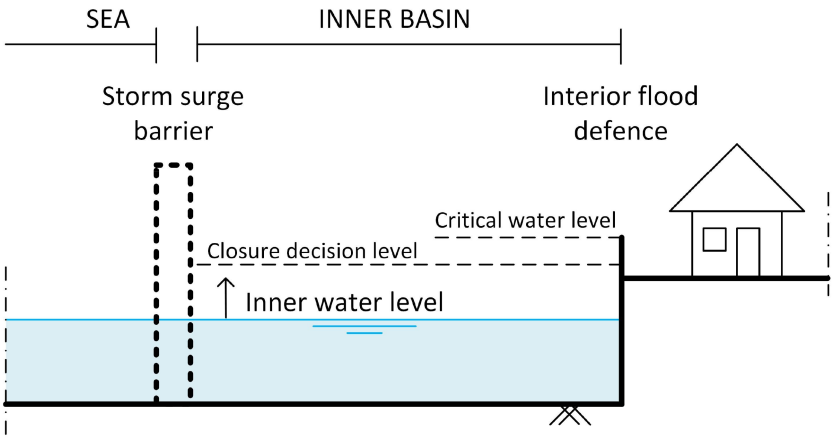

FIGURE 1 Schematic cross-section indicating the elements of a storm surge barrier flood protection system. A storm surge barrier is open in normal conditions and, therefore, indicated with a dotted line. At the interior flood defense, the critical water level is assumed to be equal to the crest level for visual clarity. The closure decision level is below the critical water level to account for water level forecast errors, the river gradient, and local wind set-up.

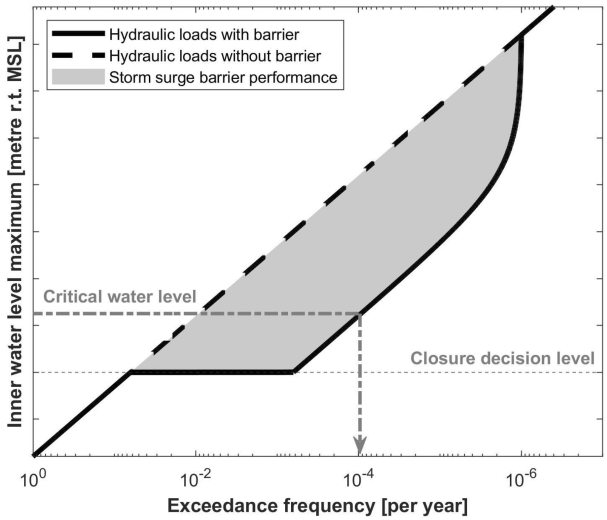

FIGURE 2 Schematic relations of exceedance frequencies of extreme water level maxima with and without a storm surge barrier based on the Maeslant barrier (Rotterdam, Netherlands), aiming at explaining the concept of "storm surge barrier performance." The method and case study describe how the hydraulic loads with a barrier are developed. Figure 12 presents how barrier failure mechanisms contribute to these hydraulic loads.

levees (USA). Figure 1 presents a principal cross-section of this flood protection system. At the critical water level, interior flood defenses are expected to fail and result in a catastrophic flood.

The role of the storm surge barrier is to prevent extreme water levels in the inner basin which exceed the critical water level of the interior defenses. Thus, the more often a storm surge barrier averts exceedances of the critical water level, the better it performs. We refer to the exceedance frequency of extreme water levels as hydraulic loads. Storm surge barrier performance is defined as the difference between the hydraulic loads with and without the barrier (see Figure 2).

Three principal failure mechanisms determine the efficacy of the flood protection system with a storm surge barrier (see Figure 3):

1. **Operational failure**: Incorrect closing or opening of the barrier due to forecasting, mechanical, electrical, and/or control errors.
2. **Structural failure**: Collapse of the barrier causing uncontrolled water flow.
3. **Hydraulic overload**: Despite successful barrier closure, water levels surpass critical water levels due to either excessive flow over and/or through the barrier, river flow accumulating behind the barrier, internal wind setup, or a combination of these effects (see Figure 3).

Mooyaart et al. (2023) show that sea level rise motivates substantial investments into storm surge barrier performance in the future. Moreover, Trace-Kleeberg et al. (2023) demonstrate the negative influence of sea level rise on the number and length of maintenance windows. This is expected to make operational failures more likely without additional measures. To determine the effectiveness of investments in storm surge barrier performance, there is a need for a method which systematically addresses all system failure mechanisms and their effect on storm surge barrier performance.

The recent scientific literature on storm surge barrier performance is usually restricted to only one or sometimes two of the three principal failure mechanisms. Christian et al. (2015) and Schlumberger et al. (2021) analyze the effect a barrier has on water levels behind the barrier. They analyze a recent event with some small alterations to that event, without discussing the frequencies of these events. Gouldby and Sayers (2009) assess flood risk behind the Thames Barrier probabilistically, but neglect barrier failures. Vader et al. (2022) argue that

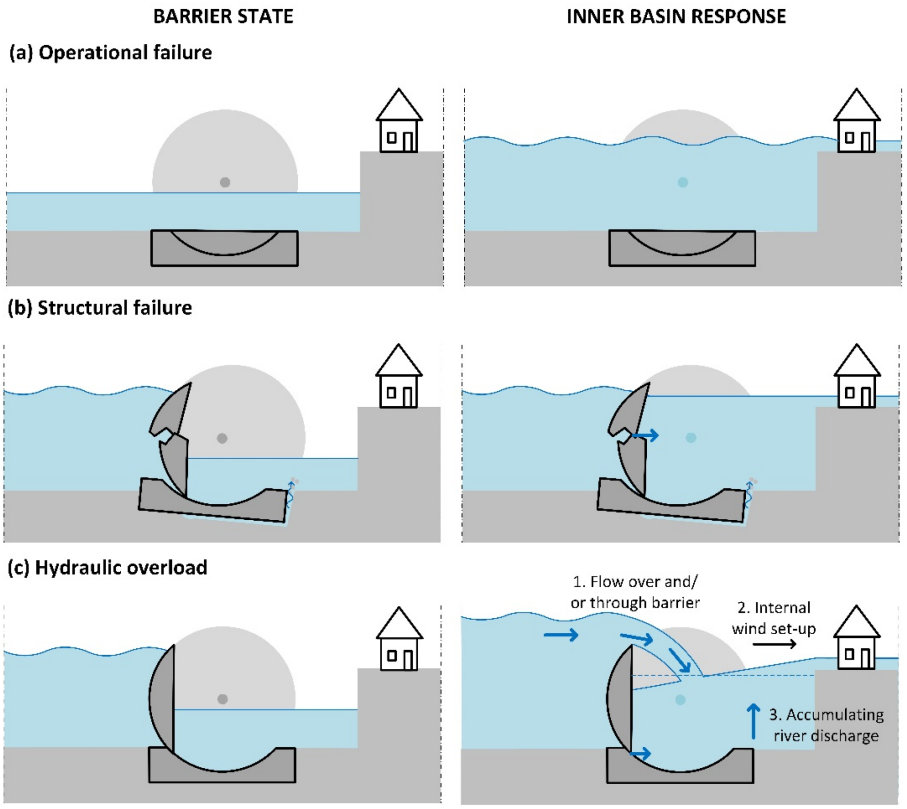

FIGURE 3 Principal system failure mechanisms. The left figure presents the barrier (failure) mode, while the right figure shows the corresponding inner basin response, which leads to exceedance of the critical water level.

structural and hydraulic overload are irrelevant to their case and, therefore, only consider operational barrier failure quantitatively. Zhong et al. (2012), Diermanse et al. (2015), and De Bruijn et al. (2022) include both operational failures and hydraulic overload due to river discharge. Their approach is also being used to determine loads for interior flood defenses in the Netherlands (Geerse, 2010). Dupuits et al. (2017) and van Berchum et al. (2019) optimize barrier flood protection systems taking into account structural failures and hydraulic overload due to barrier overflow. None of these authors consider both structural and operational failure mechanisms.

To our knowledge, the three principal failure mechanisms have only been jointly considered in design and assessment reports (Rijkswaterstaat, 1986, 2022) and a conference paper by Janssen and Jorissen (1992). The model they present is, however, difficult to reproduce, verify, and apply to other barriers. As a result, it is unclear how barrier failure mechanisms influence storm surge barrier performance. Thus, there is no systematic method to evaluate the relative importance of the three principal failure mechanisms (operational failure, structural failure, and hydraulic overload).

This paper presents a probabilistic method that evaluates storm surge barrier performance by considering all three principal failure mechanisms and the uncertainties inherent in extreme event predictions. Our method is applied to the Maeslant barrier in Rotterdam (The Netherlands) providing insight into optimizing flood protection measures.

The paper is structured as follows: Section 2 describes barrier operation and possible failures. Section 3 introduces the method to establish hydraulic loads and storm surge barrier performance. Section 4 applies the method to the Maeslant barrier (Rotterdam, Netherlands) followed by discussions and conclusions in Sections 5 and 6.

2 | BARRIER OPERATION AND FAILURE

2.1 | Barrier operation

Each storm surge barrier has two distinct modes of operation: (1) the barrier is open under normal conditions and (2) the barrier closes in case a critical high water level is forecasted. In the first mode of operation, the barrier is maintained and tested (see Kharoubi et al. (2024) for more information on asset management of these types of structures), usually taking into account seasons with a lower risk of severe weather events (Trace-Kleeberg et al., 2023).

For the second mode, storm surge barrier managers use a predefined closure strategy to operate the barrier. This strategy consists of closure criteria and control instructions. At almost all barriers, the most important closure criterion is the forecasted water level maximum, which we refer to as the *closure decision level* (h_c).

When the forecasted water level exceeds the closure decision level, the moment to start the closure is planned. Adequate time allowance to close the barrier is considered for potential operational disruptions. Closing around slack tide allows for more storage of river discharge with minimal flow conditions. However, a shorter closure time reduces the impact on navigation and tidal exchange and can reduce structural loads. In any case, the closure must be sufficiently planned ahead to communicate its timing to local stakeholders, the most important often being the port authority.

Operators employ machinery, including operating mechanisms, drives, electronic switchboards, control computers, and power supplies, to move the gates into position—a process that takes two and a half hours at the Maeslant barrier on average. Consequently, the water level at the start (*start closure level*) differs from the water level at the end (*end closure level*) especially at estuaries with a significant tidal range (>1 m). Once closed, the barrier structure, consisting of gates and foundation, withstands the hydraulic loads securing the inner basin. During the closure, the inner basin water levels are subject to falls and rises due to the abrupt tidal closure (translation waves), leakage of the barrier, river discharge, and internal wind set-up.

The barrier reopens when an equilibrium of water levels on both sides of the barrier is reached. For longer lasting storms at regions with significant astronomic tides, for instance, at the Thames Barrier (London), the barrier can close and open several times around low tide to drain the inner basin. After the storm has passed, the barrier remains open until the next storm surge event arrives.

Figure 4 illustrates the closure procedure and its effect on the inner water level h_{in}. The inner water level maximum is the highest water level during a storm surge event in the inner basin, which we indicate with a circumflex: $\widehat{h}_{in}$. In this example, the storm surge barrier operation resulted in a reduction of the inner water level maximum by approximately 1 m.

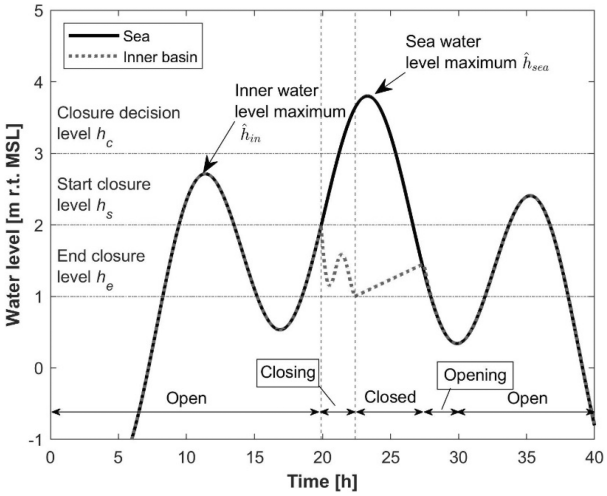

FIGURE 4 Example of inner and sea water levels during a closure procedure, based on the Maeslant barrier (Rotterdam, Netherlands). Water levels are expressed in meters relative to mean sea level (MSL).

2.2 | Barrier and system failures

In the introduction, it was stated that a failure of a storm surge barrier flood protection system is an event in which the critical water level z is exceeded. This can be caused by three principal failure mechanisms: operational, structural, and hydraulic overload failure.

Operational failures are a (partial) failure to close or to open. These failures result from decision and control errors, unavailability of staff, and malfunctioning equipment. Decision errors are more likely if the storm conditions are close to the closure criteria. Other types of operational failures are not necessarily related to the conditions at the peak of the storm.

With structural failures, storm surge barriers fail to resist the hydraulic loads. Most important hydraulic loads are the hydraulic head and wind wave impacts. They can cause the barrier to collapse, break, or undermine the foundation.

The hydraulic overload principal system failure mechanism represents scenarios where despite successful barrier operation, extreme storm surge, astronomic tide, and river conditions still cause the critical level z to be exceeded. Most barriers have considerable flow through them during a storm. The sector arms of the Maeslant barrier do not touch each other in a closed position. At the Eastern Scheldt barrier, the foundation consists of highly permeable rock mattresses. Flow through the barrier alone will not result in critical water level exceedance. However, combined with (a combination of) barrier overflow, river discharge behind the barrier, and internal wind set-up, a catastrophic flood can occur.

Finally, there are important partial failure scenarios. Closures can be too late due to an operational error, resulting in a relatively full inner basin, making critical water level exceedance more likely. At multiple gate barriers, a single gate failure results in large flow velocities

through this opening. These large flow velocities can erode bed protections or cause gates to vibrate, resulting in a structural failure.

3 | METHOD TO QUANTIFY STORM SURGE BARRIER PERFORMANCE

The section outlines the four-step method to quantify storm surge barrier performance. The four steps are the following:

1. Storm modeling
2. Barrier state modeling
3. Inner basin modeling
4. Exceedance frequency modeling.

Figure 5 provides a flow diagram of these four steps.

3.1 | Storm modeling

The aim of this first step is to establish frequency distributions of relevant (random) variables of storms. These variables can be properties of the storm itself (e.g., sea level maximum, maximum wind speed), but also the astronomic tide (e.g., tidal amplitude, tidal phase) and the river (e.g., discharge). Depending on the aim of the analysis, assumptions with respect to sea level rise can be included here. All these properties together are referred to as storm conditions S.

The more variables are considered relevant in this stage, the more complex the modeling in the next stages becomes. Therefore, it is advocated to start with the most important variable(s) and build the model onward based on the initial results.

3.2 | Barrier state modeling

In this step, system failure mechanisms are organized according to barrier states. Barrier states are the state and/or position a barrier is in during a storm, which results in a certain degree of obstruction of flow. A barrier state k can be a failed, a partially failed, or a successful state.

First, barrier states are to be defined. The analysis should at least consider two barrier states: fully open and successfully closed. Other principal barrier states which can be included are a failure to close and a structural failure. Based on the initial insights from this analysis, the number of the barrier states K can be extended. Those barrier states which are not expected to lead to critical water level exceedance are excluded.

The probability of a barrier state is related to storm conditions S. We refer to this relation as the *barrier state probability function* $P_k(S)$. These probability functions are mutually exclusive and combined encompass the entire probability space.

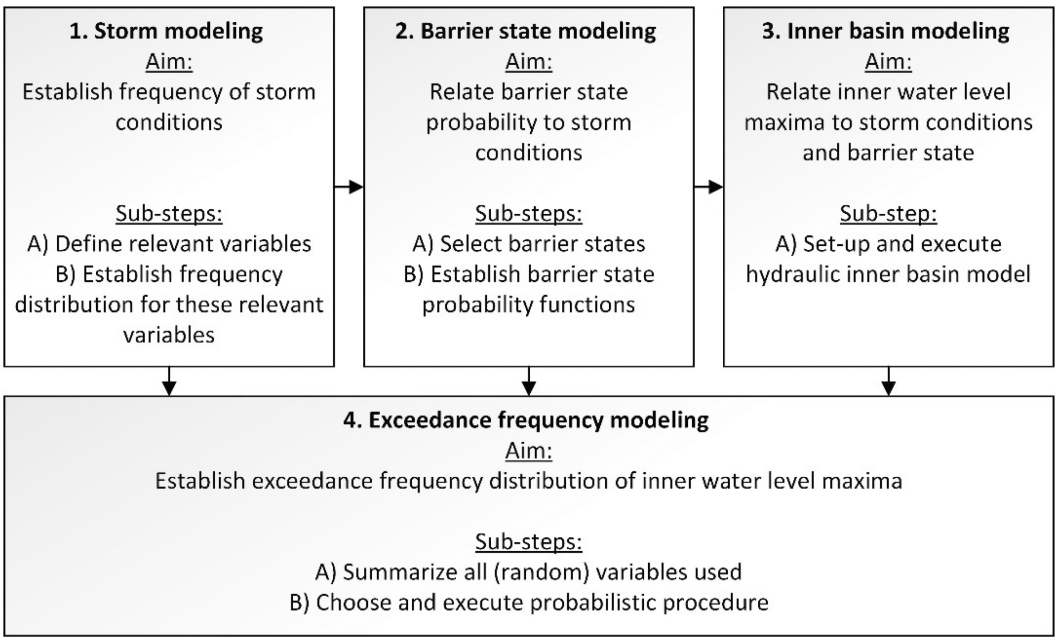

FIGURE 5 Flow diagram showing main steps to find storm surge barrier performance.

We apply an event tree to visualize the progression of events and, thereby, determine barrier states. The probability of the barrier state is the product of the conditional probabilities of the intermediate events in the event tree.

We demonstrate the development of barrier state probability functions with the event tree in Figure 6. Two types of storm events are analyzed: one which results in a flood in case the barrier remains open $\overline{A}$ and a more severe one which will result in structural or hydraulic overload failure (A). Three successful events are defined: (B) a closure decision, (C) a successful closure, and (D) hydraulic loads resisted. The failure events are indicated with a macron ‾: ($\overline{B}$) no closure decision, ($\overline{C}$) a failed closure due to mechanical, electrical, or control errors, and ($\overline{D}$) structural failure.

The frequencies of storms (events A and $\overline{A}$) are the result of the first step in this method: storm modeling. Barrier state probability functions are combinations of probability functions of Events B to D and their opposites $\overline{B}$ to $\overline{D}$. We relate the probability of successful closure decision $P(B)$ to the sea level maximum $\widehat{h}_{\text{sea}}$ [meter relative to mean sea level (m r.t. MSL)], using a normal cumulative distribution function (Φ) with the closure decision level h_c [m r.t. MSL] as a mean and the water level forecast error σ_c [m] as the standard deviation. Likewise, the (conditional) structural failure probability $P(\overline{D})$ depends on the sea level maximum $\widehat{h}_{\text{sea}}$ [m r.t. MSL] with normal distribution parameters: the mean structural fragility z_{str} [m r.t. MSL] and its standard deviation σ_{str} [m]. The constant P_{FC} is used to determine the probability of a failed closure $P(\overline{C})$ on demand. We list the barrier states in the following order: (1) open, (2) failure to close, (3) structural failure, and (4) closed and find the following barrier state probability functions:

$$P_1\left(\widehat{h}_{sea}\right) = P\left(\overline{B}\right) = 1 - \Phi\left(\frac{\widehat{h}_{sea} - h_c}{\sigma_c}\right)$$

$$P_2\left(\widehat{h}_{sea}\right) = P\left(B\overline{C}\right) = \Phi\left(\frac{\widehat{h}_{sea} - h_c}{\sigma_c}\right) \cdot P_{FC}$$

$$P_3\left(\widehat{h}_{sea}\right) = P\left(BC\overline{D}\right) = \Phi\left(\frac{\widehat{h}_{sea} - h_c}{\sigma_c}\right) \cdot (1 - P_{FC}) \cdot \Phi\left(\frac{\widehat{h}_{sea} - z_{str}}{\sigma_{str}}\right)$$

$$P_4\left(\widehat{h}_{sea}\right) = P(BCD) = \Phi\left(\frac{\widehat{h}_{sea} - h_c}{\sigma_c}\right) \cdot (1 - P_{FC}) \cdot \left\{1 - \Phi\left(\frac{\widehat{h}_{sea} - z_{str}}{\sigma_{str}}\right)\right\}.$$

Figure 7 presents these barrier state probability functions, which will later on be used in the case study. The blue line presents the probability of the barrier being open. With sea level maxima approaching the closure decision level h_c = MSL + 3.1 m, the probability of an open barrier declines. Due to the small water level forecast error $\sigma_c = 0.2$ m, it is unlikely that the barrier remains open with sea level maxima higher than MSL + 3.5 m.

The barrier state probability function of a failed closure due to mechanical, electrical, or control errors (red line) is the result of two events: a closure decision being taken and a failed closure. Until approximately MSL + 3.5 m, the probability rises as the barrier with these water level maxima can remain open due to the lack of a closure decision. For water level maxima higher than MSL + 3.5 meter, the probability of a failed closure remains constant ($P_{FC} = 1/100$ on demand).

The barrier state probability function of structural failure is the combination of three events: a closure decision, a successful closure, and a structural failure. Structural failure becomes more likely for sea level maxima above MSL + 4.0 m. Due to structural fragility (values z_{str} = MSL + 6.6 m and $\sigma_{\text{str}} = 0.5$ m), the probability of

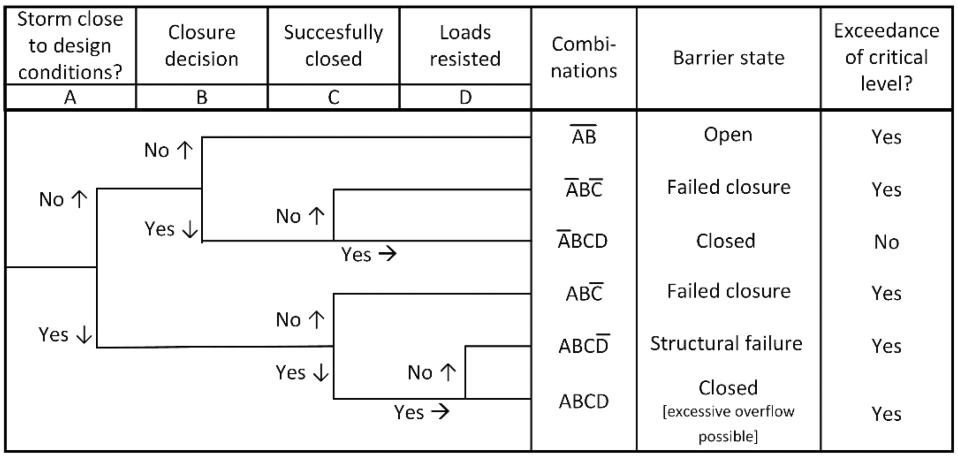

FIGURE 6 Event tree of a closure procedure. Two types of storm events are analyzed; one which results in a flood in case the barrier remains open $\overline{A}$ and a more severe one which will result in structural or hydraulic overload failure (A). For the first storm type, a structural failure cannot occur $\{P(\overline{D}) = 0\}$, and for the second type, there is always a closure decision $\{P(B) = 1\}$, and, therefore, these paths were removed.

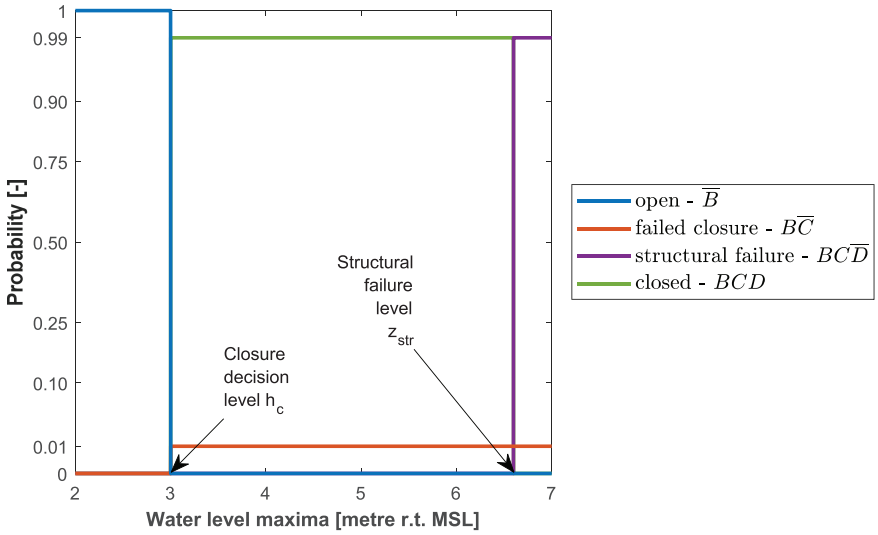

FIGURE 7 Example of barrier state probability functions used for the Maeslant barrier case study. Sea level maxima are presented in meters relative to mean sea level [m r.t. MSL]. The vertical axis was scaled using a beta distribution (2,2) to emphasize probabilities near zero and one. The symbols in the legend correspond with the events as indicated in the event tree of Figure 6.

structural failure rises to a maximum 99/100, as in 1/100 cases the closure failed due to mechanical, electrical, and/or control errors.

Successful closure is a barrier state which occurs if there is a closure decision, no failure to close, and no structural failure. As a result, for each sea level maximum, the sum of the probabilities is one.

3.3 | Inner basin modeling

The inner basin modeling aims to relate storm and river conditions and barrier states to inner water levels in front of interior flood defenses and near the barrier. Preferably, the inner basin modeling accounts for all relevant hydraulic phenomena. The inner basin model used at the Maeslant barrier covers the lower part of the Rhine and Meuse Delta, accounting for translation waves, flow through and over the barrier, river flow, internal wind set-up, water storage, the hydraulic properties of the more southerly Haringvliet sluices, and friction in channels. For the Galveston Bay, a similar model is applied to assess the feasibility of a storm surge barrier (Christian et al., 2015). However, for this paper, we use a simpler analytical model which only includes a few of the relevant hydraulic phenomena to emphasize our approach with respect to barrier state and probabilistic modeling.

Furthermore, we assume that inner water levels do not affect the probability of barrier states. Both structural loads and closure criteria can, however, be influenced by inner water levels. When there is a demand to include these effects, a feedback loop between step 3 (inner basin modeling) and step 2 (barrier state modeling) should be added.

3.4 | Exceedance frequency modeling

In this final modeling step, the exceedance frequency of the critical water level z is determined. In this section, we start to explain the method on an abstract level, after which we point out some practical issues with this abstract method. Then, we introduce the method applied for the Maeslant barrier case.

The frequency of a single event that exceeds the critical water level z is composed of (see Figure 8):

1. The frequency of a storm event $F(S)$ [per year] with properties S (= result of step 1: storm surge modeling).
2. The probability of a barrier state k given storm properties S, which are the barrier state probability functions $P_k(S)$ (= result of step 2: barrier state modeling).
3. The probability of exceedance of the critical water level z given the storm event S, the barrier state k, and inner basin properties B: $P\left(\widehat{h}_{in} > z \,|S,k,B\right)$.

Imagine that there are m possible events which exceed the critical water level. Then, the sum of the frequencies of these events amounts to the frequency of critical water level exceedance $F\left(\widehat{h}_{in} > z\right)$ [per year]:

$$F\left(\widehat{h}_{in} > z\right) = \sum_{i=1}^{m} F(S) \cdot P_k(S) \cdot P\left(\widehat{h}_{in} > z \,|S,k,B\right). \quad (1)$$

For continuous parameters, frequency and probability functions could be resolved by integration of probability density functions. However, the conditional

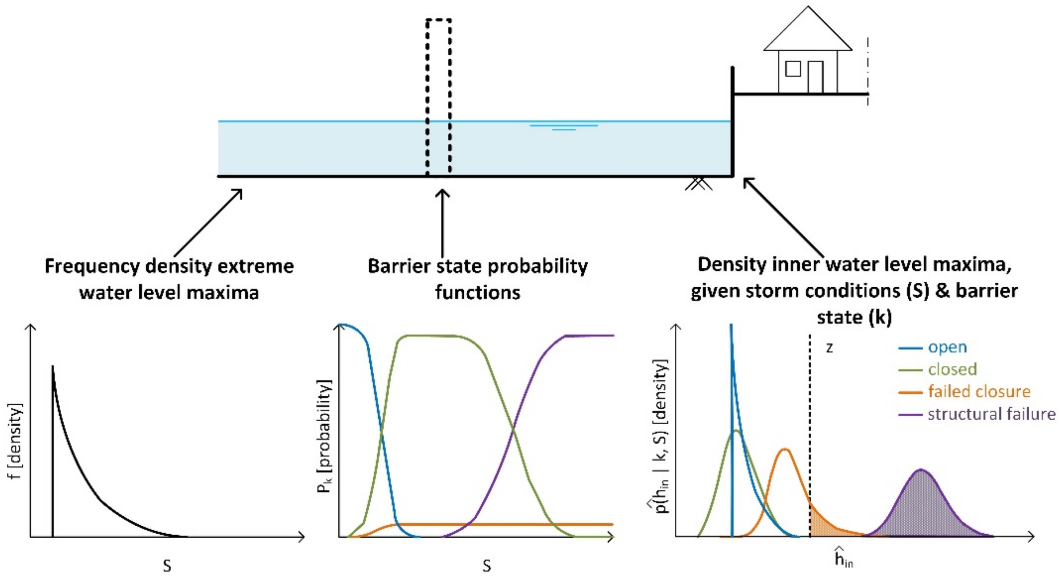

FIGURE 8 Overview of three main stochastic variables required to establish the exceedance frequency of the critical water level, corresponding to formula 2: the frequency density S, the barrier probability state functions P_k, and the density of inner water level maxima at a certain location behind the barrier given the storm conditions and barrier state $p\left(\widehat{h}_{in}|k,S\right)$. The plots in the lower panels present example functions of these main stochastic variables with a single variable describing storm severity S and four barrier states (open, closed, failed closure, and structural failure). The lower right panel indicates the critical level z with a dashed line, hatching the probability density exceeding this level. The lower right subplot is a result of multiplying the lower left and lower middle subplot, if the sea level maximum is the only variable describing the storm severity S and if the sea level maximum is equal to the inner water level maximum $\widehat{h}_{in}$, which can be a reasonable assumption for open and failed barrier states.

probability density of the inner water level $p\left(\widehat{h}_{in}|S,k,B\right)$ is an indirect result of the inner basin modeling and remains difficult to interpret. Therefore, we combine the three terms $\{f,\ P_k$ and $p\left(\widehat{h}_{in}|S,k,B\right)\}$ and introduce the partial distribution g_k, which presents the density of inner water levels for an individual barrier state. Using this approach, we can still recognize the contribution of the individual barrier states to the exceedance frequency of the critical water level, which is the main aim of this article.

The partial distributions g_k can be established with several probabilistic procedures. If there is only one random variable affecting the partial inner water level distribution, an analytical procedure can be applied. With more random variables, numerical procedures are needed. In the case study (Section 4), we demonstrate both an analytical and a numerical procedure: a Monte Carlo simulation.

The exceedance frequencies result from the integration of the partial distributions for water level maxima higher than the critical water level. The number of random variables n determines the tuple of the integral. For example, if there are three random variables, the exceedance frequency is found with a triple integral. The exceedance frequency of a critical water level for a specific barrier state $G_k\left(\widehat{h}_{in}>z\right)$[per year] is

$$G_k\left(\widehat{h}_{in}>z\right)=\int\ldots\int_{\widehat{h}_{in}>z} g_k\left\{\widehat{h}_{in}(X_1,X_2,\ldots,X_n)\right\}dX_1\ldots dX_n. \tag{2}$$

In this equation, X is a set of n random variables which affect the frequency of the inner water level maxima. The random variables encompass the storm conditions S and variables for the barrier state probability functions and could include random variables of inner basin properties.

In the final step, the exceedance frequencies of the barrier states are summed over all states to find the exceedance frequency of the critical water level $F\left(\widehat{h}_{in}>z\right)$ [per year]:

$$F\left(\widehat{h}_{in}>z\right)=\sum_{i=1}^{K} G_k\left(\widehat{h}_{in}>z\right). \tag{3}$$

This formula is also applied to examine more extreme water level maxima than the critical level z alone to find the hydraulic loads with a storm surge barrier.

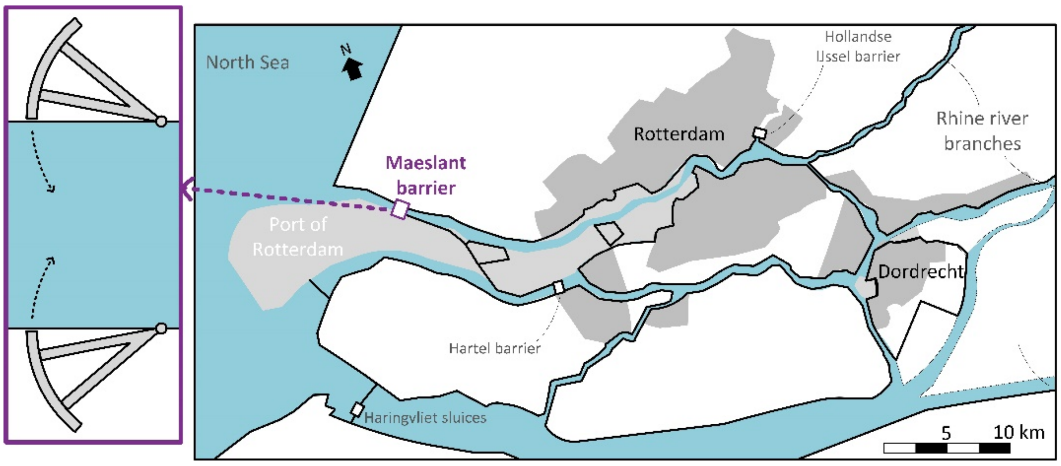

FIGURE 9 Schematic map with a top view of the Maeslant barrier (left) and the region protected by this barrier (right). Urban areas are hatched dark grey, and port areas light grey. Solid black lines are used to indicate flood defenses.

4 | ROTTERDAM CASE STUDY

4.1 | Introduction

This case study applies the method to quantify storm surge barrier performance to the Maeslant barrier in Rotterdam. We present three examples of the method: (1) an analytical probabilistic procedure with a single random variable, (2) a Monte Carlo Simulation including seven random variables, and (3) the same probabilistic procedure, but with a lower failure probability to close as a result of a performance improvement.

The Maeslant barrier was constructed to protect the cities of Rotterdam and Dordrecht against coastal floods (see Figure 9). The barrier is positioned at the New Waterway, which is the main canal connecting Rotterdam to the sea. The barrier consists of two floating sector arms. In normal conditions, these hydraulic gates are positioned in a dry dock. If the closure decision level h_c of mean sea level (MSL) + 3.0 m is predicted to be exceeded, the closure procedure starts and the gates are positioned into the New Waterway.

In this case study, we investigate the flood frequency at Rotterdam, which interior flood defenses have a critical water level z of MSL + 3.6 m.

4.2 | Analytical procedure

4.2.1 | Storm modeling

For the analytical procedure, only the sea level maximum is analyzed. Moreover, sea level rise is not accounted for, as the study aims at finding current exceedance frequencies.

Similar to Mooyaart et al. (2023), we use an exponential distribution for annual water level maxima with an annual maximum H_A of MSL + 2.1 m and a decimal height H_B of 0.75 m. Thus, the probability density function of this distribution is

$$f_{\text{sea}}\left(\widehat{h}_{\text{sea}}\right) = \frac{\ln 10}{H_B} \cdot 10^{\frac{\widehat{h}_{\text{sea}} - H_A}{H_B}}. \quad (4)$$

4.2.2 | Barrier state modeling

We define four barrier states: open, failed closure, structural failure, and successful closure. A failure to reopen again is excluded as its likelihood of leading to critical level exceedance is low. The event tree in Figure 6 was used to arrange barrier states.

We applied the following barrier state probability functions (see Figure 10):

1. **Open**: If the predicted sea level maximum is lower than the closure decision level h_c, the barrier remains open. For all other sea level maxima, a closure decision is taken.
2. **Failed closure**: If the sea level maximum exceeds the closure decision level, the probability of a failed closure is $P_{\text{FC}} = 1/100$ on demand (Dutch Law on Water, 2021) regardless of the sea level maximum.
3. **Structural failure**: The structural design was based on hydraulic loads with a return period of 1,000,000 years (Janssen et al., 1994). A sea level maximum of MSL +6.6 m corresponds to this return period. We assume that if this level z_{str} is exceeded,

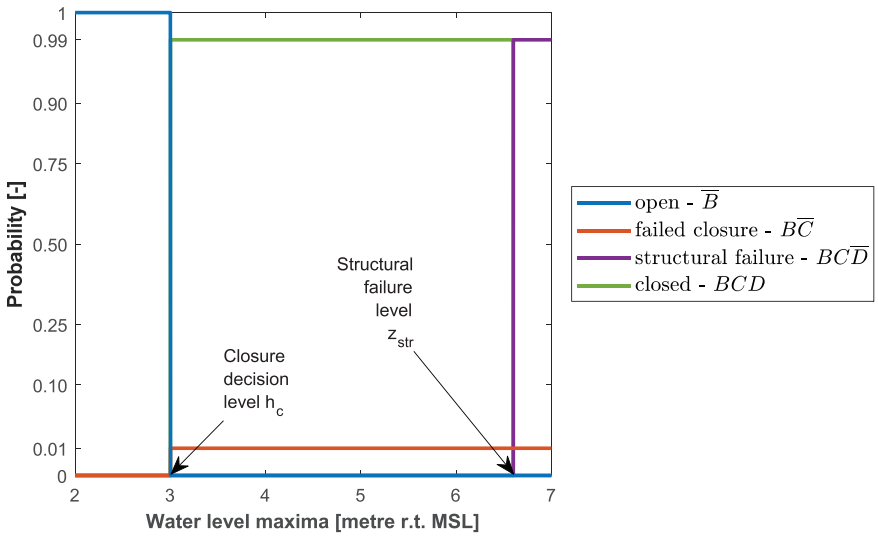

FIGURE 10 Barrier state probability functions for the analytic procedure. The barrier remains open below the closure decision level (blue line) and always fails structurally above the structural failure level z_{str}. Between these closure decisions and structural failure levels, the barrier closes successfully with a rate of 99/100 on demand and thus fails in 1/100 demands. The vertical axis was scaled using a beta distribution (2,2) to emphasize probabilities near zero and one. The symbols in the legend correspond with the events as indicated in the event tree of Figure 6.

the barrier fails structurally and that no structural failure occurs below this level.

4. **Successful closure**: In all other cases, closure is successful, hence $P_4(h_c \leq \widehat{h}_{sea} < z_{str}) = 99/100$ on demand.

4.2.3 | Inner basin model

In case of successful closure, the barrier obstructs the flow. For the analytical procedure, we assume that all inner water level maxima result in the closure decision level. Thus, we neglect the role of river discharge and barrier overflow.

For the open and failed closure mode, the storm surge can freely enter the New Waterway. We assume that the flow is unobstructed in case of structural failure as well. With unobstructed flow (open, failed closure, and structural failure barrier states) sea level maxima are equal to inner water level maxima. As Rotterdam is located near the Maeslant barrier, this is a realistic assumption. We demonstrate that for the failed closure barrier state, this approach leads to similar results as previous studies, which use a more accurate inner basin model.

4.2.4 | Exceedance frequency modeling

With the assumption of the previous paragraph, the partial density function g_k is merely the product of the barrier probability functions and the sea level density functions for the open and failed barrier states (1: open, 2: failed closure, and 3: structural failure):

$$g_k\left(\widehat{h}_{in}\right) = f_{sea}\left(\widehat{h}_{sea}\right) \cdot P_k\left(\widehat{h}_{sea}\right), \tag{5}$$

in which P_k is the barrier state probability function and f_{sea} is the probability density of sea water level maxima [per year per meter].

For the closed barrier state (barrier state 4), the closure frequency F_4 is added at the closure decision level:

$$g_4\left(\widehat{h}_{in} = h_c\right) = F_4 = \int f_{sea}\left(\widehat{h}_{sea}\right) \cdot P_4\left(\widehat{h}_{sea}\right) d\widehat{h}_{sea}\,. \tag{6}$$

Equation 2 is used to determine the exceedance frequency of the critical water level per barrier state. Equation 3 finds the hydraulic loads with a storm surge barrier.

4.2.5 | Results

Figure 11 shows the partial densities of the four barrier states. The open barrier state density is equal to the density without a barrier until the closure decision level. The closed barrier state has a frequency equal to the closure frequency at the closure decision level, which results in an infinitely high density at this water level.

The densities of the barrier failure mechanisms are much smaller and, therefore, plotted on two separate panels. The density of the failed closure is a factor of a hundred lower than without a barrier. Above MSL + 6.6 m, the combination of structural failure and a failure to close results in a density equal to the density without a barrier.

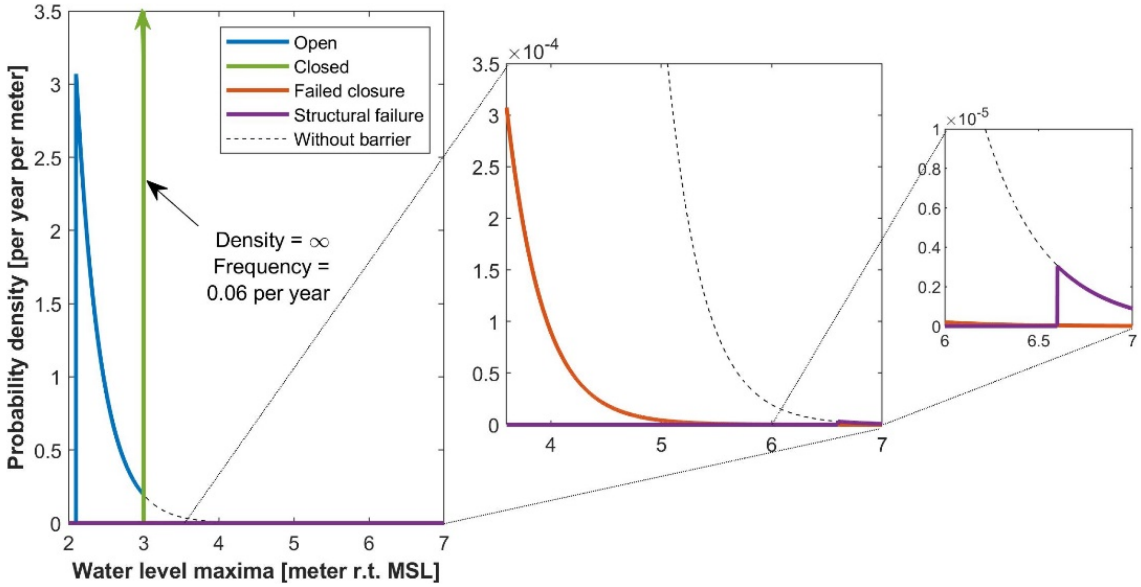

FIGURE 11 Probability density of water level maxima at Rotterdam with and without a barrier. Colored lines are used to indicate the contribution of specific barrier states to the density, while a thin dashed black line shows the density without a barrier. The left figure shows the density over the entire range of water level maxima. The middle figure presents the density for water levels higher than the critical water level (MSL + 3.6 m), while the right figure zooms in even smaller probability densities for water levels exceeding MSL + 6 m.

Figure 12 presents the results with exceedance frequencies on the horizontal axis in reverse direction. In this example, the critical water level can only be exceeded if the barrier is in one of two barrier states (failed closure or structural failure). The exceedance frequency with the failed closure is 10^{-4} per year, which is similar to what was found in a previous study (HKV, 2006). Exceedance of the critical level due to structural failure is a hundred times less likely: 10^{-6} per year.

Storm surge barrier performance can be found by comparing the hydraulic loads with and without the barrier. The figure shows that between the closure decision and structural failure level, the hydraulic load is affected by the storm surge barrier. The exceedance frequency of MSL + 5.1 m provides insight into how the model functions. At this water level, the exceedance frequency of a failed closure and a structural failure are equal (10^{-6} per year). The sum of the exceedance frequencies of all barrier states 2×10^{-6} is the exceedance frequency with a storm surge barrier (see Equation 3). Below MSL + 5.1 m, failure to close is most important for storm surge barrier performance, while for higher levels structural failure is.

The open and closed barrier states contribute to lower extreme water levels. The closed barrier state has a constant exceedance frequency until the closure decision level, equal to the closure frequency. The open barrier state exceedance frequency approaches an asymptote equal to the closure decision level. When combined, these two barrier states result in a hydraulic load equal to the hydraulic load without a barrier.

4.3 | Monte Carlo simulation

For the second probabilistic procedure, we adopt the following:

- More variables describing the storm conditions are included; the sea level maximum is split into storm surge and astronomic tide. Moreover, river discharge is considered which can accumulate behind the barrier.
- The same four barrier states are applied; however, we use barrier probability functions which include uncertainty with respect to forecasting and structural failure (see Figure 7).
- A slightly more sophisticated, but still simplified, inner basin model is applied to account for the effect of accumulating river discharge, which is elaborated upon in Section 4.3.1.

The properties of the additional variables describing storm conditions and the barrier probability functions are presented in Table 1.

4.3.1 | Inner basin modeling

For all barrier states, we model the inner water level h_{in} [meter relative to mean sea level (MSL)] during a storm. Table 1 presents the meaning, dimension, and value of these variables. The inner water level is constituted of three components: the storm surge h_{storm}, the

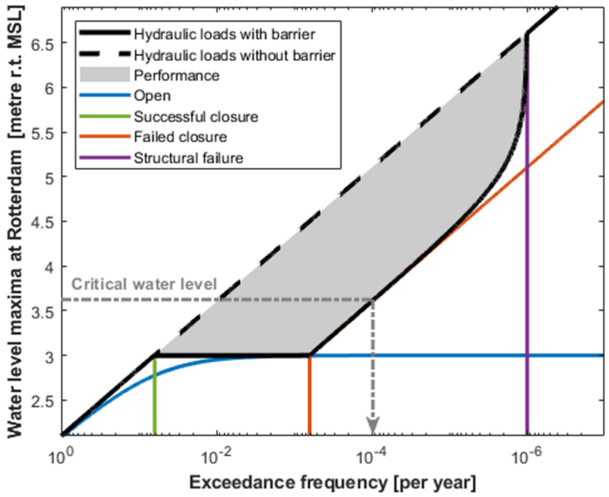

FIGURE 12 Hydraulic loads at Rotterdam with and without a barrier using the analytical procedure expressed in meters relative to mean sea level (MSL). Exceedance frequencies of the yearly water level maximum (10^0) are dominated by the storm surge barrier remaining open (blue line). With higher water level maxima, it becomes less likely that the barrier remains open (blue line), and, therefore, the blue line reaches an asymptote equal to the closure decision level. This blue line (open barrier) does not follow the black dashed line (without a barrier), as with a barrier there are also other barrier states which result in exceedances of these extreme water level maxima. The barrier closes successfully with a frequency of 6/100 per year, all resulting in an extreme water level maximum equal to the closure decision level (green line). For extreme water level maxima above the closure decision level, a failure to close (red line) occurs every once in a hundred times and, hence, exceedance frequencies of inner water level maxima are 100 times as low as without a barrier. Structural failures (purple) occur with extreme water level maxima above the structural failure level of MSL + 6.6 m. The hydraulic loads with a barrier (black) are the sum of the inner water level maxima exceedance frequency of the four barrier states (open, closed, failed closure, and structural failure).

astronomic tide h_{tide}, and the river component h_{river}. Using similar assumptions regarding storm patterns and river influence as Zhong et al. (2012), we use the following equation for the open barrier states:

$$\begin{aligned} h_{\text{in}}(t) &= h_{\text{barrier}}(t) = h_{\text{storm}}(t) + h_{\text{tide}}(t) + h_{\text{river}}(t) \\ h_{\text{storm}}(t) &= \zeta_{\text{storm}} \cdot \cos^2\left\{\frac{\pi}{T_{\text{storm}}} \cdot \left(t - \frac{1}{2} \cdot T_{\text{storm}}\right)\right\} \\ h_{\text{tide}}(t) &= \zeta_{\text{tide}} \cdot \sin\left\{\frac{2 \cdot \pi}{T_{\text{tide}}} \cdot (t - \varphi)\right\} \\ h_{\text{river}}(t) &= \frac{1}{2 \cdot g} \cdot \left(\frac{\frac{8}{9} \cdot Q_{\text{Rhine}}}{\mu \cdot A_{\text{mouth}}}\right)^2. \end{aligned} \tag{7}$$

For all barrier states, we neglect any water level differences between Rotterdam and the Maeslant barrier $\{h_{\text{in}}(t) = h_{\text{barrier}}(t)\}$.

The start of the closure takes place at the start closure level h_s (MSL + 2 m) closest before the first exceedance of the closure decision level, corresponding to the closure procedure of the Maeslant barrier.

Multiple effects cause the water level to drop after the start of the closure (negative translation wave, tidal phase difference between Maeslant barrier, Haringvliet and the rest of the lower rivers, and internal wind set-up). To account for these effects, we use an end closure level h_e of MSL + 1 m.

River flow and overflow over the barrier cause the inner basin to rise gradually during closure. River flow spreads over a wide area: Besides the New Waterway also the larger Haringvliet Lake. We use a single basin approximation to estimate the water level rise, considering the entire area (300 km^2, based on publicly available data on lake sizes and estimates using Google Maps). We ignore the effect that for higher water levels (h_{in} > MSL + 2.5 m), the storage area rapidly increases. Like Zhong et al. (2012), we only consider the Rhine flow, neglecting the smaller Meuse flow and account for one-ninth of the flow being diverted upstream through the IJssel to the Northern part of the Netherlands.

In this model, we neglect flow through the barrier and only consider barrier overflow Q_{overflow} [m^3/s]. We use within the hydraulic engineering field commonly applied formula (Ministerie van Verkeer en Waterstaat, 1990):

$$Q_{\text{overflow}}(t) = c \cdot W \cdot \{h_{\text{barrier}}(t) - z\}^{1.5}. \tag{8}$$

To find the water level rise due to overflow, again the single basin approximation is applied. However, we assume that the water spreads over a smaller area (A_{overflow} = 50 km^2). The inner water level with barrier closure is then:

$$h_{\text{in,closed}} = h_{\text{ECL}} + \frac{8/9 \cdot Q_{\text{Rhine}}}{A_{\text{Rhine}}} \cdot (t - t_{\text{EC}}) + \sum_{t_{\text{EC}}}^{t} \frac{Q_{\text{overflow}}}{A_{\text{overflow}}} \cdot \Delta t, \tag{9}$$

in which t_{EC} is the time at the end of the closure and Δt is the time step, which was taken at 1200 s (20 min).

For extremely high river discharges (>6000 m^3/s), the barrier closes around low tide. However, this specific closure procedure was excluded from the inner basin model

TABLE 1 Properties of variables of Monte Carlo simulation.

Variable	Symbol	Unit	Distr.	μ	σ	Source
Storm surge	ζstorm	m	Exp.	1.2	0.75	Annual maximum minus average tidal range
Storm duration	Tstorm	s	Logn.	12.2	0.11	Deltares (2017)
River discharge	Q_{river}	m^3/s	Logn.	7.7	0.5	Zhong et al. (2012)
Tidal phase	φ	s	Unif.	0	44,712	
Closure decision level	h_c	m*	Normal	3.1	0.2	HKV (2011)
Prob. failed closure	PFC		Bern.	1/100		
Structural fragility	z_{str}	m*	Normal	6.6	0.5	
Tidal amplitude	ζ_{tide}	m	Det.	0.9		Semi-diurnal component (M2) of tide
Tidal period	T_{tide}	s	Det.	44,712		
Start closure level	hs	m*	Det.	2		Janssen et al. (1994)
End closure level	he	m*	Det.	1		assumption is based on a small number of hydraulic model run outputs
River flow section	μA_{mouth}	m^2	Det.	3620		Zhong et al. (2012)
Rhine basin	A_{Rhine}	km^2	Det.	300		Based on satellite images and publicly available data of lake sizes
Crest level barrier	z_{crest}	m*	Det.	5		Janssen et al. (1994)
Overflow constant	c	m/s^2	Det.	1.9		Ministerie van Verkeer en Waterstaat (1990)
Width barrier	W	m	Det.	360		Janssen et al. (1994)
Overflow basin	$A_{overflow}$	km^2	Det.	50		Based on satellite images and publicly available data of lake sizes
Grav. acc.	g	m/s^2	Det.	10		

Note: The lognormal cumulative distribution has the following structure: $\frac{1}{2}\left[1+\text{erf}\left(\frac{\ln x-\mu}{\sigma\sqrt{2}}\right)\right]$. For the exponential distribution, the value μ corresponds to the annually exceeded water level and σ is the decimal height. For the uniform distribution, μ and σ are the lower and upper bound, respectively.
Abbreviations: Det., deterministic; Exp., exponential; Logn., lognormal; m*, meter relative to mean sea level. Unif., uniform.

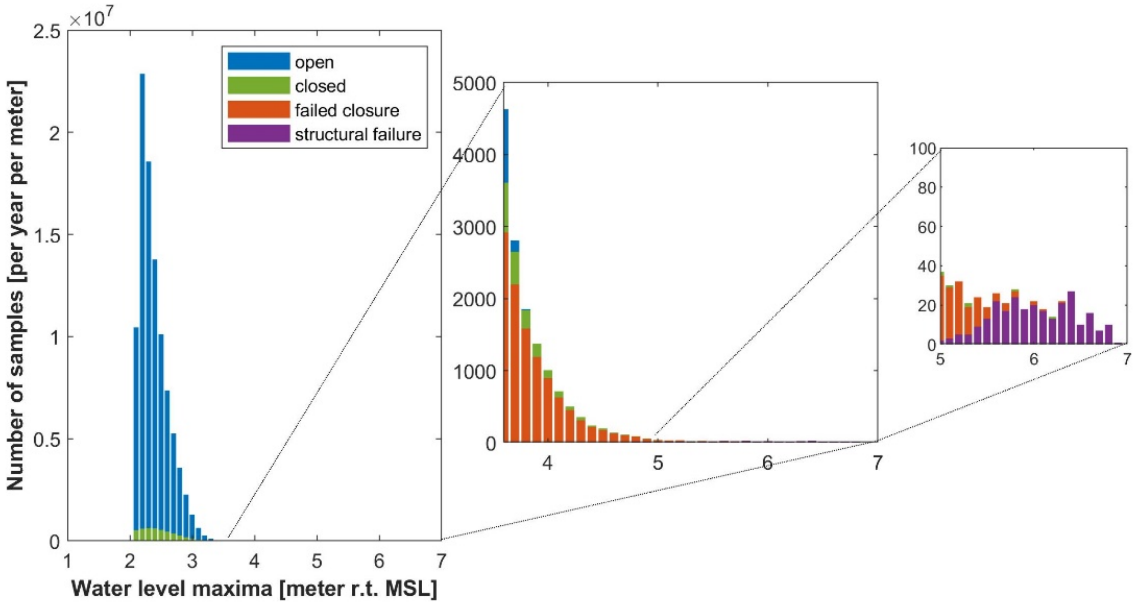

FIGURE 13 Histograms with the number of samples from the Monte Carlo simulation (10^8 samples) that resulted in an inner water level maximum (bins 0.1 m). The left figure presents all samples and the middle figure presents those which exceed the critical water level. The right figure zooms in on water levels exceeding MSL + 5 m.

as it had little effect on inner water level maxima. Very extreme river discharges were maximized until 18,000 m^3/s to account for upstream river flooding.

4.3.2 | Exceedance frequency modeling

Table 1 presents the properties of all variables applied in this case. A Monte Carlo simulation is performed where 10^8 random samples are taken from the seven distributions presented in Table 1. For each sample of all distributions, the inner basin model is run to find the inner water level maximum. The inner water level maxima are grouped in the four barrier states: open, closed, failed closure, and structural failure.

4.3.3 | Results

Figure 13 shows the number of samples within bins of 0.1 m. Most samples result in an open situation. Closures occur often as well, but barrier failures are rarely drawn. Exceedances of the critical water level of MSL + 3.6 m are, however, mostly the result of barrier failures to close.

Figure 14 presents the hydraulic loads with and without a barrier. The exceedance frequency of the critical water level is 1.4×10^{-4} per year with a barrier and 1.0×10^{-2} per year without a barrier. The storm surge barrier performance is mainly influenced by the possibility of a failed closure (1×10^{-4} per year) but is significantly affected by the open (1×10^{-5} per year) and closed (2×10^{-5} per year) barrier states as well. Although structural fragility was included, structural failure remains an unlikely cause for exceedance of the critical water level (2×10^{-6} per year).

Overflowing events almost never result in exceedance of the critical water level. We analyzed severe overtopping events but found that the difference between end closure and critical water level provides sufficient storage for overflow even in rare cases.

Comparing both methods (analytical and Monte Carlo), the Monte Carlo approach revealed additional scenarios where open and closed barrier states lead to critical level exceedances. For the open and closed modes, the exceedance frequency is about 2×10^{-5} per year. The failed closure partial distribution is similar to the analytical solution, which was expected because the same input was used. The structural failure frequency is slightly higher at the critical water level than the analytical method (2×10^{-6} per year) as the possibility of structural failure with lower levels was included.

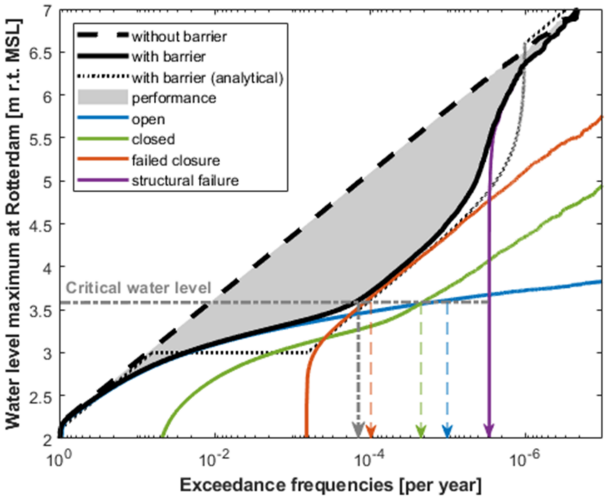

FIGURE 14 Hydraulic loads with and without a barrier with a Monte Carlo simulation with 10^8 samples. The colored lines indicate the exceedance frequencies of the inner water levels for each barrier state. The open (blue) and closed (green) barrier states occur most often, typically resulting in extreme water level maxima below the critical level. Forecast errors at the open barrier state and high river discharges accumulating behind the barrier at the closed barrier state can cause the critical water level to be exceeded, with frequencies of about 10^{-5} per year (see dashed arrows). Failed closures and structural failures occur less frequently than open and closed barrier states, but have relatively high water level maxima. Near and above the critical level, failed closures occur at a constant rate of once in a hundred relative to the hydraulic loads without a barrier. Structural failures occur at the higher extreme water level maxima and due to the assumed structural fragility, this curve approaches the hydraulic loads without a barrier in a curved manner. The hydraulic load with a barrier is the sum of the four exceedance frequencies of the barrier states. The critical water level of the flood defenses behind the barrier is indicated with a grey dash-dot line.

4.4 | Performance improvement

As a final example, we only adapt the probability of a failed closure from 1/100 to 1/1000 on demand. This lower probability is the result of a performance improvement of the Maeslant barrier such as an additional barrier which was proposed by Rijcken et al. (2023).

Figure 14 (left) presents the exceedance frequencies of extreme water levels with the performance improvement. Compared to the previous example, the partial distribution of the failed closure has moved to the right, having exceedance frequencies exactly a factor of 10 lower. Due to this shift, the hydraulic overload failure mechanism has the highest contribution to the exceedance frequency of the critical level (48%).

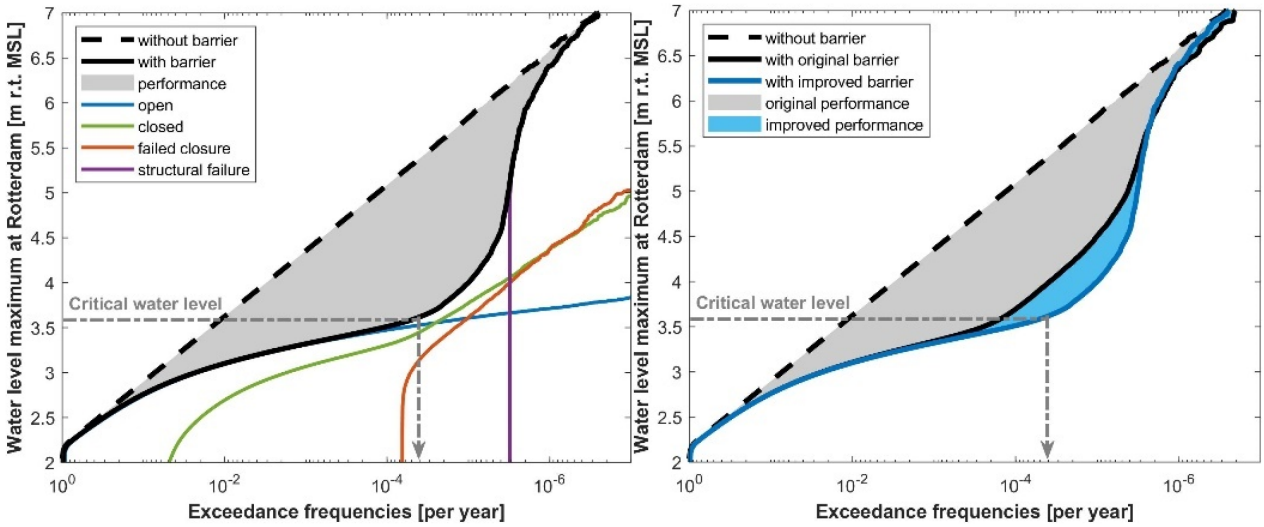

FIGURE 15 Exceedance frequencies with a performance improvement, which has lowered the probability of failed closure from 1/100 to 1/1000 on demand. Differences in performance for frequencies below 10^{-6} per year are caused by the inaccuracy of the Monte Carlo simulation for lower frequencies.

TABLE 2 Overview of exceedance frequencies of the critical water level [per year] for the analytical procedure, the Monte Carlo simulation, and the performance improvement which has lowered the probability of a failed closure from 1/100 to 1/1000 on demand.

Failure mechanism	Analytical procedure	Monte Carlo simulation	Performance improvement
Operational f., forecast error	0	1×10^{-5}	1×10^{-5}
Hydraulic overload[a]	0	2×10^{-5}	2×10^{-5}
Operational f., failed closure	1×10^{-4}	1×10^{-4}	1×10^{-5}
Structural failure	1×10^{-6}	2×10^{-6}	2×10^{-6}
Total	1.0×10^{-4}	1.4×10^{-4}	4.2×10^{-5}

[a]Exceedance of the critical level is mainly (>99%) caused by high river discharges accumulating behind the barrier, the contribution due to excessive barrier overflow is negligible.

Figure 15 (right) and Table 2 reference show that the exceedance frequency of the critical level was lowered from 1.4×10^{-4} to 4.2×10^{-5} per year. Thus, a performance improvement of the failed closure of a factor 10 resulted in a flood frequency of three times as low.

5 | DISCUSSION

This study introduces a method for assessing the relative importance of various principal failure mechanisms in storm surge barrier systems. The method is transparent as it explicitly quantifies the performance of the storm surge barriers and shows how failure mechanisms contribute.

The method has several applications: It can detect weak spots of the coastal protection, as barriers often have a crucial position, and, thus, their most important failure mechanism is likely to be such a weak spot. The method can also be used to aid decision-making with respect to effectiveness of maintenance and upgrades. For instance, if a more advanced forecasting system is considered, the method can indicate whether forecasting errors are the most important failure mechanism. If so, together with the economic optimization model by Mooyaart et al. (2023), the method can indicate the return on investment of a more advanced forecasting system.

Furthermore, the method is highly flexible. It can incorporate more detailed models to become more accurate, such as more advanced inner basin and structural models. The method can consider many barrier states, which might be useful for storm surge barriers with multiple gates (Eastern Scheldt barrier [the Netherlands] has 62) or inner basins that are affected by multiple structures (West Closure Complex [New Orleans, LA, USA] contains 11 pumps and a sector gate). More complex system failure mechanisms can be incorporated such

as a barrier failure due to a collapse of the bed protection. In this scenario, the barrier gate(s) fail partially resulting in high flow velocities in the remaining opening.

Another example of a factor that could drive outcomes for other barriers is the role of astronomical spring tides. For instance, at the Thames Barrier, sea level maxima dominated by astronomical spring tides can be well-predicted in advance and are not necessarily accompanied with bad weather. Storm surge dominated sea level maxima have unfavorable conditions and, thus, higher failure probabilities. It could be relevant to include this effect in the barrier state modeling.

Probabilistic methods such as those presented in this paper explicitly model uncertainty. Storm surge barriers have to deal with relatively large uncertainties as storm surges are rare, there are only a few dozens of storm surge barriers worldwide,[1] each of them has unique characteristics and no barrier failures have been reported yet. As a result of this data sparsity, results are generally difficult to validate. Adding more complex models as suggested in the previous paragraph, can increase this validation challenge.

In this method, we analyze the effect storm surge barriers have on inner water levels. For some barrier systems, the role of wind waves and flood duration is important as well. In Venice, for instance, the closure decision level is lower with more severe wind, as the inner waves are higher and are likely to cause more damage. If those parameters are relevant, the hydraulic load and subsequent performance definition and the corresponding probabilistic method should include these parameters.

In the case study, we applied two probabilistic techniques. The analytical technique was efficient and for failed barrier states equally accurate. The Monte Carlo simulation was especially valuable with the closed barrier state, with more variables affecting inner water level maxima. An optimal balance between model efficiency and accuracy could be to use different probabilistic techniques per barrier state.

6 | CONCLUSIONS

This study introduces a general method for evaluating how structural, operational, and hydraulic overload failures in storm surge barriers affect the critical level exceedance frequency in the inner basin. The applicability of the method was demonstrated on the basis of a case study of the Maeslant barrier which protects Rotterdam (Netherlands). Applied to the Maeslant barrier in Rotterdam, the method identified the most significant failure mechanism: operational failure due to mechanical, electrical, or control errors. Structural failure, hydraulic overload, and forecast errors become more important if the probability of a failed closure is lowered by a factor of 10. Thus, we proved the method to be able to assess multiple types of system failure mechanisms.

Given that coastal flood risk is rising, the method helps to get better insight into the weak spots of storm surge barriers in protecting the hinterland. Storm surge barrier managers can use the method to identify potential risk reduction measures and assess their effectiveness. Moreover, this method can be used to evaluate storm surge barrier improvements in coastal defense strategies against sea level rise.

ACKNOWLEDGMENTS

The authors would like to acknowledge the financial support from the Directorate General of Public Works and Water Management (Rijkswaterstaat), the Netherlands. Yara Kharoubi, Hans Janssen, and the two independent reviewers are thanked for their review of the manuscript. Discussions with Nick Zegers, Krijn Saman, Eddy van de Ketterij, Veerle Sperber, Wilbert Huijbregtse, and Jesse Simons contributed to the development of the method presented in this paper.

DATA AVAILABILITY STATEMENT

Data sharing not applicable to this article as no datasets were generated or analysed during the current study.

SUPPORTING INFORMATION

The Matlab code developed for this article is available at https://github.com/LeslieMooyaart/Storm-surge-barrier-performance/

ORCID

L. F. Mooyaart https://orcid.org/0000-0003-2571-4045

ENDNOTE

[1] Mooyaart and Jonkman (2017) identified 18. I-storm (2021) presents an overview with 33 barriers using a wider definition than used in this article, but only 5 countries (Belgium, England, Italy, The Netherlands, and USA). Trace-Kleeberg et al. (2023) suggest that there are over 50 storm surge barriers.

REFERENCES

Christian, J., Fang, Z., Torres, J., Deitz, R., & Bedient, P. (2015). Modeling the hydraulic effectiveness of a proposed storm surge barrier system for the, modeling the hydraulic effectiveness of a proposed storm surge barrier system for the Houston ship channel during hurricane events. *Natural Hazards Review*, *16*, 04014015. https://doi.org/10.1061/(asce)nh.1527-6996.0000150

De Bruijn, K. M., Diermanse, F. L., Weiler, O. M., De Jong, J. S., & Haasnoot, M. (2022). Protecting the Rhine-Meuse delta against

sea level rise: What to do with the river's discharge? *Journal of Flood Risk Management*, *15*(3), 1–15. https://doi.org/10.1111/jfr3.12782

Deltares. (2017). Stochasts for flood protection assessment (Dutch: Basisstochasten WBI-2017). Technical Reports.

Diermanse, F. L., De Bruijn, K. M., Beckers, J. V., & Kramer, N. L. (2015). Importance sampling for efficient modelling of hydraulic loads in the Rhine–Meuse delta. *Stochastic Environmental Research and Risk Assessment*, *29*, 637–652. https://doi.org/10.1007/s00477-014-0921-4

Dupuits, E. J., Schweckendiek, T., & Kok, M. (2017). Economic optimization of coastal flood defense systems. *Reliability Engineering and System Safety*, *159*, 143–152. https://doi.org/10.1016/j.ress.2016.10.027

Dutch Law on Water (Dutch: Waterwet), (2021), https://wetten.overheid.nl/BWBR0025458/ 2021-01-01.

Geerse, C. (2010). Summary of probabilistic models for fresh water *(Dutch:Overzichtsdocument probabilistische modellen zoete wateren Hydra-VIJ, Hydra-B en Hydra-Zoet)*. Technical Report HKV and Rijkswaterstaat.

Gouldby, B., & Sayers, P. (2009). A methodology for regional-scale flood risk assessment. *Water Management*, *162*, 347–348. https://doi.org/10.1680/wama.2009.00084

HKV. (2006). *Achterlandstudie Maeslantkering*. Hydra-B. Technical Report.

HKV. (2011). Hydra-Zoet for the freshwater systems in The Netherlands probabilistic model for the assessment of dike heights. Technical Report December. http://publicaties.minienm.nl/download-bijlage/23355/hydra-zoet-for-the-fresh-water-system-in-the-netherlands.pdf

I-storm. (2021). *Storm surge barriers within the I-STORM network*. Retrieved August 27, 2024 https://www.i-storm.org/initiatives/downloads

Janssen, J., van Ieperen, A., Kouwenhoven, B., Nederend, J., Pruijssers, A., & de Ridder, H. A. (1994). The design and construction of the new waterway storm surge barrier in The Netherlands. In 28th PIANC world congress -Seville, Spains.

Janssen, J. P., & Jorissen, R. E. (1992). Integrating forecast effects and operational behaviour in designing the Rotterdam storm surge barrier. In *Floods and flood management. Fluid mechanics and its applications*. Springer. https://doi.org/10.1007/978-94-011-1630-5_22

Kharoubi, Y., van den Boomen, M., van den Bogaard, J., & Hertogh, M. (2024). Asset management for storm surge barriers: How and why? *Structure and Infrastructure Engineering*, *16*(5), 1–15. https://doi.org/10.1080/15732479.2024.2391034

Ministerie van Verkeer en Waterstaat. (1990). *Design Formulae for Hydraulic*. (Dutch: rekenregels voor Waterbouwkundig Ontwerpen). Technical Reports.

Mooyaart, L. F., Bakker, A. M. R., van den Bogaard, J. A., Rijcken, T., & Jonkman, B. (2023). Economic optimization of coastal flood defence systems including storm surge barrier closure reliability. *Journal of Flood Risk Management*, *16*, 12904. https://doi.org/10.1111/jfr3.12904

Mooyaart, L. F., & Jonkman, S. N. (2017). Overview and design considerations of storm surge barriers. *Journal of Waterway, Port, Coastal, and Ocean Engineering*, *143*, 06017001. https://doi.org/10.1061/(asce)ww.1943-5460.0000383

Rijcken, T., Mooyaart, L. F., Oerlemans, C., Van der Ziel, F., Borghans, J., Botterhuis, T., Winden, A. V., Jorissen, R. E., & Kok, M. (2023). It takes two to tango with sea level rise. *TU Delft DeltaLinks*, 1–16. https://flowsplatform.nl/{#}/it-takes-two-to-tango-with-sea-level-rise-1682542508929

Rijkswaterstaat. (1986). *Design documents Eastern Scheldt barrier [Dutch: Ontwerpnota Oosterscheldekering]*. Technical Report. https://repository.tudelft.nl/islandora/object/uuid%3Adda73a61-a199-4e6b-ad8c-6dd8a68bf147

Rijkswaterstaat. (2022). *Legal assessment trajectory 2018, Eastern Scheldt barrier [Dutch: Wettelijke beoordeling traject 218, Oosterscheldekering]*. Technical report.

Schlumberger, J., Ferrarin, C., Jonkman, S. N., Loaiza, A. D., Antonini, A., & Fatori, S. (2021). Developing a framework for the assessment of current and future flood risk in Venice, Italy. *Natural Hazards and Earth System Sciences Discussions*, *22*(7), 1–30. https://doi.org/10.5194/nhess-22-2381-2022

Trace-Kleeberg, S., Haigh, I. D., Walraven, M., & Gourvenec, S. (2023). How should storm surge barrier maintenance strategies be changed in light of sea level rise? A case study. *Coastal Engineering*, *184*, 104336.

Vader, H., Bakker, A. M., Jonkman, S. N., van den Boomen, M., van Baaren, E., & Diermanse, F. L. (2022). A framework for assessing the remaining life of storm surge barriers. *Structure and Infrastructure Engineering*, *20*(12), 2022–2034.

van Berchum, E. C., Mobley, W., Jonkman, S. N., Timmermans, J. S., Kwakkel, J. H., & Brody, S. D. (2019). Evaluation of flood risk reduction strategies through combinations of interventions. *Journal of Flood Risk Management*, *12*, 1–17. https://doi.org/10.1111/jfr3.12506

Zhong, H., van Overloop, P. J., van Gelder, P., & Rijcken, T. (2012). Influence of a storm surge Barrier's operation on the flood frequency in the rhine delta area. *Water (Switzerland)*, *4*, 474–493. https://doi.org/10.3390/w4020474

SUPPORTING INFORMATION

Additional supporting information can be found online in the Supporting Information section at the end of this article.

How to cite this article: Mooyaart, L. F., Bakker, A. M. R., van den Bogaard, J. A., Jorissen, R. E., Rijcken, T., & Jonkman, S. N. (2025). Storm surge barrier performance—The effect of barrier failures on extreme water level frequencies. *Journal of Flood Risk Management*, *18*(1), e13048. https://doi.org/10.1111/jfr3.13048